Proc. of the European Safety and Reliability Conference (ESREL 2026)
Edited by José C. Matos, Paulo B. Lourenço, Michael Beer, Daniel Oliveira, Edoardo Patelli, Hélder S. Sousa, Rui A. Silva and Monica Santamaria
© 2026 ESREL 2026 Organizers. *Published by* Research Publishing, Singapore.
doi: 10.3850/ESREL2026061419_esrel26-p26380-cd

A Coupled Rigid-Flexible Dynamics and Stochastic Process Model for Wear Prediction in Multi-bar Linkages

Shaoyang Du[a], Chao Zhang[a,b,c], Shaoping Wang[a,b,c], Yaohui Lu[a,d], Rentong Chen[a,c,e]

[a] *School of Automation Science and Electrical Engineering, Beihang University, Beijing, P.R. China.*
[b] *Ningbo Institute of Technology, Beihang University, Ningbo, P.R. China.*
[c] *Science and Technology on Aircraft Control Laboratory, Beihang University, Beijing, P.R. China.*
[d] *The Institute of Microelectronics of Seville, IMSE-CNM, CSIC/University of Seville, Sevilla, Spain.*
[e] *State Key Laboratory of Mechanical Transmission for Advanced Equipment, Chongqing University, Chongqing, P.R. China.*

Accurately predicting wear in multi-bar linkages is essential for their long-term performance and high reliability. The progressive wear of joints often leads to a loss of kinematic precision and even catastrophic failure. However, conventional methods, which rely on deterministic models, neglect the stochastic nature of wear that arises under dynamic contact conditions. Consequently, these models may fail to accurately predict the wear process under the dynamics of rigid–flexible coupling framework. Moreover, they overlook the non-linearity of the wear degradation process. To overcome these limitations mentioned above, this paper presents an integrated wear prediction method to capture randomness and nonlinear behavior under the influence of rigid–flexible coupling dynamics. Firstly, a rigid–flexible coupling dynamic model is developed by combining screw theory with the Floating Frame of Reference Formulation. Screw theory describes the rigid-body motion and joint constraints, while the Floating Frame of Reference Formulation characterizes the elastic deformations of flexible links. Secondly, the wear model is established based on Archard's theory. The Gamma process, taking into account multiple uncertainties, is used to describe the wear degradation process under dynamic contact conditions. Thirdly, an integrated framework combining dynamic model and multiple wear degradation processes is established. Within this framework, the geometric clearance and contact characteristics of all joints are progressively updated to update the wear rate in a step-by-step manner. Finally, the effectiveness of the proposed method is demonstrated through a case study involving a spatial Revolute-Spherical-Spherical-Revolute four-bar linkage. Results demonstrate a significant improvement in wear prediction accuracy over conventional deterministic models. By capturing both the random and non-linear characteristics of degradation, the proposed method provides a reliable tool for the wear prediction of rigid–flexible coupling mechanisms.

Keywords: Rigid–flexible coupling dynamics, Joint wear prediction, Archard wear model, Gamma process, Multi-bar linkages.

1. Introduction

Multi-bar linkages are widely employed in high precision motion systems, including landing gear and control surfaces in aerospace vehicles, as well as manipulators in industrial robots. However, under harsh loads and complex environmental conditions, wear in the joints of multi-bar linkages is inevitable, leading to increased joint clearance and altered contact conditions. These factors introduce uncertainty, making the wear process difficult to predict. It is essential to construct a high accuracy wear prediction model to ensure safety and reliability of multi-bar linkages systems (Gao et al., 2024).

Kinematic analysis constitutes the foundation for the motion characterization and control of spatial multi-bar linkages. Conventionally, Karhan and Bingül (2025) employed the Denavit–Hartenberg (D–H) parameter method for kinematic modeling of multi-bar systems, while Müller (2018) adopted screw theory to describe spatial motion and joint constraints. To account for elastic deformations, Liu et al. (2024) developed a rigid–flexible coupling model, extending purely kinematic frameworks to capture link flexibility effects. Among rigid–flexible coupling formulations, the Floating Frame of Reference

Formulation (FFRF) and the Absolute Nodal Coordinate Formulation (ANCF) are commonly employed (Tang et al., 2024; Zhai et al., 2023). Sun and Hu (2024) further demonstrated that for spatial linkages undergoing large overall motions with small elastic deformations, FFRF effectively decouples rigid-body kinematics from modal coordinates, improving computational efficiency while maintaining accuracy. However, most existing approaches do not account for progressive joint wear and its interaction with system dynamics, leading to degraded motion accuracy and altered dynamic behavior.

Wear evolution is typically represented by Archard's wear equation, while classical contact mechanics adopts Hertzian contact theory to estimate contact pressures under elastic deformation (Muratović et al., 2024; Pawlus and Reizer, 2025). Wear exhibits significant variability; deterministic models often fail to capture such complexity (Springis and Boiko, 2025; Kolawole et al., 2024), motivating stochastic modeling approaches (Dykha et al., 2025). However, most existing models neglect the coupled feedback between progressive wear and evolving contact geometry, introducing cumulative prediction errors over extended operation.

Motivated by the above observations, this work proposes a physics-informed stochastic wear prediction framework for spatial multi-bar linkages. The main contributions are as follows:

(1) To characterize contact and mechanical behavior of multi-bar linkages, a multibody model integrating screw theory with FFRF is developed, enabling evaluation of contact kinematics and load redistribution in closed-loop mechanisms.
(2) To accurately model progressive wear degradation, a contact driven update scheme based on Archard's law is formulated, where accumulated wear depth is fed back to joint geometry to capture evolving contact states.
(3) To quantify the uncertainties induced by wear degradation, a physics-informed Gamma process is developed to model stochastic wear accumulation with load-dependent randomness, yielding probabilistic life predictions.

The rest of this paper is organized as follows. Section 2 develops the rigid–flexible coupling model using screw theory and FFRF. Section 3 presents wear modeling for clearance joints. Section 4 introduces the physics-informed Gamma process and coupled framework. Section 5 validates the proposed framework on an RSSR mechanism. Section 6 concludes.

2. Rigid–Flexible Dynamics

2.1. *Screw-Theory Kinematics*

Multi-bar linkages are modeled using screw theory for rigid body kinematics, which provides a singularity free, coordinate independent representation of spatial multibody motion and joint constraints(Murray et al., 1994). Each joint k is characterized by a twist $\boldsymbol{\xi}_k \in \mathbb{R}^6$ with rotational part $\boldsymbol{\omega}_k$ and translational part $\boldsymbol{v}_k$:

$$\boldsymbol{\xi}_k = \begin{bmatrix} \boldsymbol{\omega}_k \\ \boldsymbol{v}_k \end{bmatrix}, \tag{1}$$

where $\boldsymbol{v}_k = -\boldsymbol{\omega}_k \times \boldsymbol{q}_k$ with $\boldsymbol{q}_k$ being the coordinates of a point on the axis.

For closed-loop mechanisms, the kinematic chain is decomposed into two branches a and b from the base to a common end body. Using the Product of Exponentials formula, the configurations of the end body are

$$\begin{aligned} \boldsymbol{T}_a(\boldsymbol{q}_r) &= \left(\prod_{k \in \mathcal{A}} e^{\hat{\boldsymbol{\xi}}_k \theta_k} \right) \boldsymbol{T}_{a0}, \\ \boldsymbol{T}_b(\boldsymbol{q}_r) &= \left(\prod_{k \in \mathcal{B}} e^{\hat{\boldsymbol{\xi}}_k \theta_k} \right) \boldsymbol{T}_{b0}, \end{aligned} \tag{2}$$

where $\mathcal{A}$ and $\mathcal{B}$ are the joint index sets, $\boldsymbol{q}_r$ collects the joint variables θ_k, $\hat{\boldsymbol{\xi}}_k \in \mathbb{R}^{4\times4}$ is the matrix representation of twist $\boldsymbol{\xi}_k$ in the Lie algebra $se(3)$ via the hat map $\hat{(\cdot)}$, and $\boldsymbol{T}_{a0}, \boldsymbol{T}_{b0}$ are the reference configurations of the end body on branches a and b, respectively. The closed-loop constraint $\boldsymbol{T}_a = \boldsymbol{T}_b$ is enforced via

$$\boldsymbol{\Phi}_{\text{rigid}}(\boldsymbol{q}_r) = \text{Log}\big(\boldsymbol{T}_b^{-1}\boldsymbol{T}_a\big)^{\vee} = \boldsymbol{0}_{6\times1}. \tag{3}$$

where $\text{Log}(\cdot)^{\vee} : SE(3) \rightarrow \mathbb{R}^6$ denotes the Lie group logarithm followed by the vee map, extracting the six twist coordinates from a group element.

2.2. *Elastic Deformation*

The Floating Frame of Reference Formulation (FFRF) (Shabana, 1997) is adopted to model elastic deformation of flexible links. FFRF decouples rigid body kinematics from small elastic deformations via a floating reference frame, enabling efficient simulation while maintaining accuracy for links with small strain. Let P denote a material point on body i, with global position $\boldsymbol{r}^i_P \in \mathbb{R}^3$:

$$\boldsymbol{r}^i_P(\boldsymbol{q}^i) = \boldsymbol{R}^i + \boldsymbol{A}^i \left(\bar{\boldsymbol{r}}^i_P + \boldsymbol{u}^i_f\right), \tag{4}$$

where $\boldsymbol{R}^i \in \mathbb{R}^3$ and $\boldsymbol{A}^i \in \mathbb{R}^{3\times 3}$ are the translation and rotation of the body frame, $\bar{\boldsymbol{r}}^i_P \in \mathbb{R}^3$ is the undeformed local position of P, and $\boldsymbol{u}^i_f \in \mathbb{R}^3$ is the elastic displacement.

Let $\boldsymbol{q} = [\boldsymbol{q}_r^T, \boldsymbol{q}_f^T]^T$ denote the generalized coordinates, collecting both rigid and flexible components. The velocity of point P is obtained by differentiation:

$$\dot{\boldsymbol{r}}^i_P = \boldsymbol{J}^i_P(\boldsymbol{q})\,\dot{\boldsymbol{q}}, \tag{5}$$

where $\boldsymbol{J}^i_P(\boldsymbol{q}) \in \mathbb{R}^{3\times n_q}$ is the translational Jacobian, which maps generalized velocities to local point velocities.

The equations of motion for the rigid–flexible system are written in the form

$$\boldsymbol{M}(\boldsymbol{q})\ddot{\boldsymbol{q}} + \boldsymbol{h}(\boldsymbol{q},\dot{\boldsymbol{q}}) + \begin{bmatrix} \boldsymbol{0} & \boldsymbol{0} \\ \boldsymbol{0} & \boldsymbol{K}_{ff}\boldsymbol{q}_f + \boldsymbol{D}_{ff}\dot{\boldsymbol{q}}_f \end{bmatrix} = \boldsymbol{Q}_{\text{ext}} + \boldsymbol{Q}_{\text{con}} + \boldsymbol{\Phi}_{\boldsymbol{q}}^T\boldsymbol{\lambda}. \tag{6}$$

where $\boldsymbol{M}(\boldsymbol{q})$ is the mass matrix, $\boldsymbol{h}(\boldsymbol{q},\dot{\boldsymbol{q}})$ collects inertial and velocity-dependent terms, $\boldsymbol{K}_{ff}$ and $\boldsymbol{D}_{ff}$ are the modal stiffness and damping matrices, $\boldsymbol{Q}_{\text{ext}}$ is the external force vector, $\boldsymbol{\Phi}_{\boldsymbol{q}}$ is the constraint Jacobian with Lagrange multipliers $\boldsymbol{\lambda}$, and $\boldsymbol{Q}_{\text{con}}$ represents contact forces at clearance joints.

The normal force and tangential force at contact pair k are denoted by $\boldsymbol{F}_{n,k}$ and $\boldsymbol{F}_{t,k}$. The generalized contact force vector is obtained from the virtual work principle:

$$\boldsymbol{Q}_{\text{con}} = \sum_{k\in\text{contacts}} \boldsymbol{J}^T_{rel,k}\left(\boldsymbol{F}_{n,k} + \boldsymbol{F}_{t,k}\right). \tag{7}$$

The matrix $\boldsymbol{J}_{rel,k} \in \mathbb{R}^{3\times n_q}$ is the relative translational Jacobian at the contact point. For contact between bodies i and j, it is defined as

$$\boldsymbol{J}_{rel,k} = \boldsymbol{J}^i_{P,k} - \boldsymbol{J}^j_{P,k}, \tag{8}$$

where $\boldsymbol{J}^i_{P,k}$ and $\boldsymbol{J}^j_{P,k}$ are the translational Jacobians of the contact points on bodies i and j.

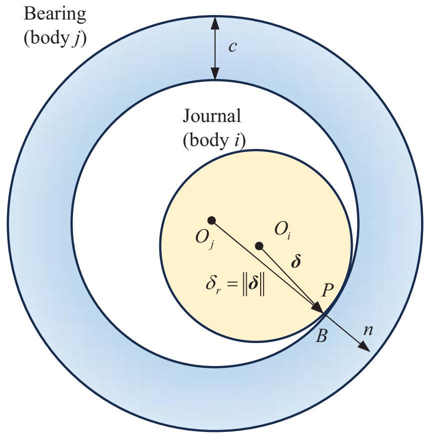

Fig. 1. Contact geometry and force decomposition of a revolute joint with clearance under journal–bearing contact conditions

3. Wear Modeling for Clearance Joints

3.1. *Contact Geometry and Kinematics*

As shown in Fig. 1, wear and assembly eccentricity cause an offset between the journal and bearing centers, creating a localized contact region. The normal direction governs contact pressure, while the tangential direction determines sliding velocity and wear rate.

Let P and B denote contact points on the mating bodies, with global positions $\boldsymbol{r}_P$ and $\boldsymbol{r}_B$ given by:

$$\boldsymbol{r}_P = \boldsymbol{R}^i + \boldsymbol{A}^i\boldsymbol{u}^i_P, \quad \boldsymbol{r}_B = \boldsymbol{R}^j + \boldsymbol{A}^j\boldsymbol{u}^j_B, \tag{9}$$

where $\boldsymbol{u}^i_P$ and $\boldsymbol{u}^j_B$ are the local position vectors of the contact points on bodies i and j, respectively.

The relative position vector is defined as

$$\boldsymbol{\delta} = \boldsymbol{r}_B - \boldsymbol{r}_P. \tag{10}$$

The normal gap function $g_n(\boldsymbol{q},t)$ is defined using the radial clearance c and the eccentricity distance $\delta_r = \|\boldsymbol{\delta}\|$:

$$g_n = c - \delta_r. \tag{11}$$

The contact state is determined by the sign of the normal gap. Separation corresponds to $g_n > 0$. Contact corresponds to $g_n \leq 0$. The penetration depth is defined as

$$\delta_p = -g_n = \delta_r - c. \tag{12}$$

The unit normal vector at the contact interface is defined as

$$\boldsymbol{n} = \frac{\boldsymbol{\delta}}{\delta_r}. \tag{13}$$

The contact force is decomposed into normal and tangential components: the normal force provides compliance and dissipation, while the tangential force represents friction.

3.2. *Contact Force Model*

The normal contact force is modeled using the Lankarani–Nikravesh formulation (Lankarani and Nikravesh, 1990), which accounts for energy dissipation through a hysteresis damping term proportional to the penetration depth and impact velocity:

$$F_n = K\,\delta_p^{n_H} + D\,\dot{\delta}_p, \tag{14}$$

where K is the contact stiffness, n_H is the Hertzian exponent, δ_p is the penetration depth, and $\dot{\delta}_p$ is the penetration rate. The damping coefficient D is defined by

$$D = \frac{3K(1-c_r^2)\delta_p^{n_H}}{4\dot{\delta}^{(-)}}. \tag{15}$$

The parameter c_r is the coefficient of restitution and $\dot{\delta}^{(-)}$ is the initial impact velocity.

The tangential friction force is modeled by a velocity-dependent Coulomb law:

$$\boldsymbol{F}_t = -\mu(\|\boldsymbol{v}_t\|)\,F_n\,\frac{\boldsymbol{v}_t}{\|\boldsymbol{v}_t\|}, \tag{16}$$

where $\mu(\|\boldsymbol{v}_t\|)$ is the velocity-dependent friction coefficient and the tangential relative velocity $\boldsymbol{v}_t$ in the contact plane is

$$\boldsymbol{v}_t = (\boldsymbol{I} - \boldsymbol{n}\otimes\boldsymbol{n})\,(\dot{\boldsymbol{r}}_B - \dot{\boldsymbol{r}}_P)\,, \tag{17}$$

where $\boldsymbol{I}$ is the 3×3 identity matrix and $\boldsymbol{n}\otimes\boldsymbol{n}$ denotes the outer product (rank-1 projection matrix onto the contact normal direction).

The point velocities $\dot{\boldsymbol{r}}_P$ and $\dot{\boldsymbol{r}}_B$ are obtained from the Jacobian relations in the rigid–flexible kinematics.

3.3. *Archard Wear Law*

Wear evolution is modeled using Archard's law (Archard, 1953), where the wear rate is proportional to the normal contact load and sliding velocity. The wear depth rate at the interface is

$$\dot{h}(\boldsymbol{q},t) = \frac{k_{\text{wear}}}{H_{\text{mat}}}\,\|\boldsymbol{v}_t\|\,\sigma_n\,\mathcal{I}(g_n), \tag{18}$$

where k_{wear} is the wear coefficient, H_{mat} is the material hardness, σ_n is the normal contact stress, and $\mathcal{I}(g_n)$ is a contact indicator.

A force-based form is obtained by using an equivalent contact area A_{contact} and the normal force F_n:

$$\dot{h}(t) = \frac{k_{\text{wear}}}{H_{\text{mat}}\,A_{\text{contact}}}\,F_n(t)\,\|\boldsymbol{v}_t(t)\|\,\mathcal{I}(g_n). \tag{19}$$

The indicator function represents the contact state and is defined as

$$\mathcal{I}(g_n) = \begin{cases} 1, & g_n \leq 0, \\ 0, & g_n > 0. \end{cases} \tag{20}$$

4. Physics-Informed Gamma Process for Wear Degradation

4.1. *Stochastic Wear Process*

Let $\{W(t),\, t \geq 0\}$ denote the cumulative wear depth, modeled as a non-homogeneous Gamma process to capture degradation randomness while preserving physical consistency. The Gamma process is chosen for its monotone non-decreasing sample paths and positive increments, which are physically consistent with irreversible cumulative wear (van Noortwijk, 2009).

For the discrete wear update at time instants $\{t_n,\, n = 0, 1, \ldots\}$, the wear increment $\Delta W_n = W(t_{n+1}) - W(t_n)$ follows a Gamma distribution:

$$\Delta W_n \sim \text{Gamma}(\alpha \cdot \Delta\Lambda_n,\, \beta), \tag{21}$$

where $\alpha > 0$ is the shape parameter governing intrinsic variability, $\beta > 0$ is the rate parameter, and $\Delta\Lambda_n$ is the physics-based wear increment over the interval $[t_n, t_{n+1}]$, defined as:

$$\Delta\Lambda_n = \int_{t_n}^{t_{n+1}} \dot{h}(\tau)\, d\tau, \tag{22}$$

where $\dot{h}(\tau)$ is the instantaneous wear rate computed from Eq. (19).

Consequently, the mean and variance of the stochastic wear increment are derived as:

$$\mathbb{E}[\Delta W_n] = \frac{\alpha \cdot \Delta\Lambda_n}{\beta}, \tag{23}$$

$$\mathrm{Var}[\Delta W_n] = \frac{\alpha \cdot \Delta\Lambda_n}{\beta^2}. \tag{24}$$

4.2. *Parameter Estimation*

The parameters α and β are unknown and must be estimated from historical degradation data via maximum likelihood estimation. Given M wear trajectories, the increments $\Delta W_{m,n}$ and the corresponding physics-based increments $\Delta\Lambda_{m,n}$ are collected. The log-likelihood function is

$$\mathcal{L}(\alpha,\beta) = \sum_{m=1}^{M} \sum_{n} \Big[(\alpha\Delta\Lambda_{m,n} - 1) \log \Delta W_{m,n} - \beta\Delta W_{m,n} + \alpha\Delta\Lambda_{m,n} \log\beta - \log\Gamma(\alpha\Delta\Lambda_{m,n}) \Big]. \tag{25}$$

where $\Gamma(\cdot)$ denotes the Euler gamma function (not to be confused with the Gamma process).

The parameter estimates $\hat{\alpha}$ and $\hat{\beta}$ are obtained by maximizing Eq. (25) subject to $\alpha, \beta > 0$, which is equivalent to solving the first-order conditions:

$$\frac{\partial\mathcal{L}}{\partial\alpha} = 0, \quad \frac{\partial\mathcal{L}}{\partial\beta} = 0. \tag{26}$$

The Newton-Raphson method is employed to solve this nonlinear system numerically, yielding $\hat{\alpha}$ and $\hat{\beta}$ for subsequent wear prediction via Eq. (21).

4.3. *Coupled Simulation Framework*

The overall workflow is illustrated in Fig. 2. The framework operates on two time scales: a fine scale with step Δt for dynamics integration, and a coarse scale with interval Δt_n for geometry updates. At each wear step n, the multibody system is solved to obtain contact forces and sliding velocities. The increment $\Delta\Lambda_n$ is then computed via Archard's law (Eq. (19)), and a stochastic increment ΔW_n is sampled from Eq. (21). The clearance is updated as $c_{n+1} = c_n + \gamma\,\Delta W_n$, where c_n is the effective joint clearance radius at step n and γ converts wear depth into clearance increment, forming a closed-loop feedback that progressively alters contact conditions until the failure threshold W_{crit} is reached.

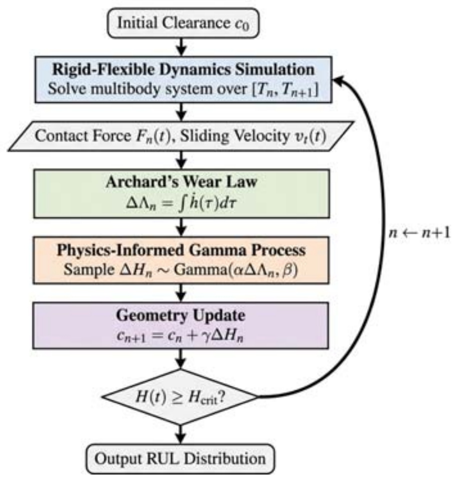

Fig. 2. Coupled simulation framework integrating rigid–flexible dynamics, physics-informed Gamma process, and geometric feedback for progressive wear prediction.

5. Case Study

An RSSR spatial linkage (Fig. 3) is employed to validate the proposed framework. The mechanism comprises four links: R1 and R4 are base-mounted revolute joints, while R2 and R3 are spherical joints forming the spatial closed loop. To capture rigid–flexible coupled wear evolution, the following assumptions are adopted:

(1) **Flexible link**: Link 2 is modeled as a flexible body, while Links 1, 3, and the ground are treated as rigid bodies.

(2) **Wear site**: Joint wear is considered only at revolute joint R1. An initial radial clearance c_0 is assigned to R1 to represent manufacturing tolerances.

The physical, geometric, and wear-related parameters are summarized in Table 1.

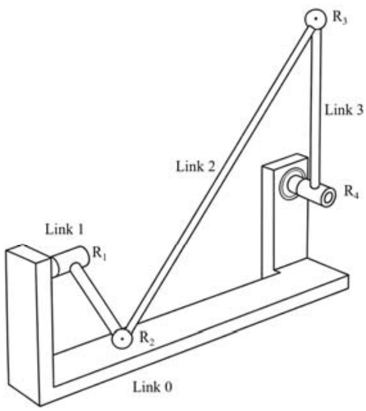

Fig. 3. Configuration of the RSSR spatial mechanism

The mechanism is driven by a constant-speed rotational excitation with a frequency of 2 Hz. For validation purposes, an equivalent multibody dynamic model is constructed in Adams, which serves as a high-fidelity reference for comparing key dynamic responses and joint load histories.

Fig. 4 shows the joint contact force over one motion cycle, exhibiting nonlinear time-varying behavior: rapid decay initially, followed by significant amplification near the end configuration, reflecting the mechanism's influence on joint loading. The proposed method agrees well with Adams simulations in both magnitude and trend, validating the contact dynamics model.

Fig. 5 shows the circumferential wear depth distribution at Cycle 10, 20, and 30 for three models: Deterministic (Det), the proposed rigid–flexible coupled stochastic model (Prop), and Adams validation (Adams). Local peaks appear at specific angular positions, indicating that periodic high load contact governs the wear process. The proposed model captures subtle angular shifts in peak positions relative to the deterministic baseline, with

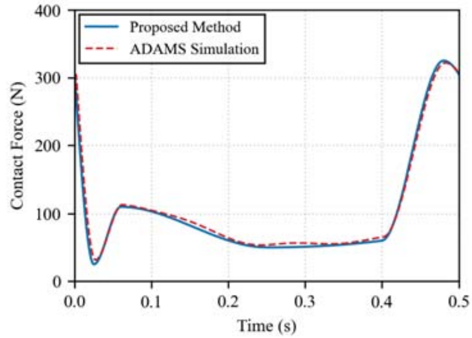

Fig. 4. Time history of joint contact force comparison between the proposed method and Adams simulation

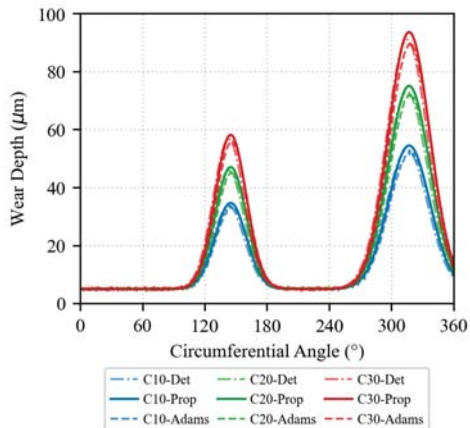

Fig. 5. Circumferential distribution of joint wear depth at different operating cycles

offsets consistent with Adams simulations. This shift arises from rigid–flexible coupling effects on contact kinematics, which the deterministic model cannot reproduce.

Fig. 6 shows the predicted RUL probability distributions for three stochastic models: the proposed model, Baseline 1 without rigid–flexible coupling, and Baseline 2 without wear evolution feedback. The proposed model exhibits the narrowest distribution centered closest to the ground truth, indicating superior prediction accuracy and appropriate uncertainty quantification. Both baseline models yield distributions shifted toward higher RUL values, with Baseline 1 exhibiting the

Table 1. Physical and wear-related parameters of the RSSR spatial mechanism

Category	Parameter	Symbol	Value
Geometric parameters	Link 1 length	L_1	120 mm
	Link 2 length	L_2	420 mm
	Link 3 length	L_3	260 mm
	Link 2 cross-section radius	r_2	6 mm
Material properties	Young's modulus	E	210 GPa
	Poisson's ratio	ν	0.30
	Density	ρ	$7850\,\mathrm{kg/m^3}$
Flexible modeling	Modal truncation order of Link 2	n_f	6
Joint geometry	Initial radial clearance of R1	c_0	$10\,\mu\mathrm{m}$
Contact parameters	Equivalent elastic modulus	E^*	115 GPa
	Equivalent Poisson's ratio	ν^*	0.30
Wear model parameters	Wear coefficient	k_{wear}	1.0×10^{-8}
	Contact hardness	H_{mat}	3.5 GPa
Failure criterion	Critical wear depth	W_{crit}	$80\,\mu\mathrm{m}$

Table 2. Remaining useful life prediction statistics

Metric	Proposed Model	Baseline 1	Baseline 2
Mean (cycles)	24.8	25.7	25.4
Std. (cycles)	0.75	1.10	0.85
COV (%)	3.02	4.28	3.35
Error (%)	-1.20	$+2.39$	$+1.20$

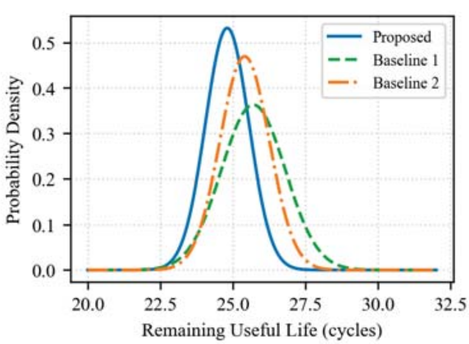

Fig. 6. Probability density function of the predicted remaining useful life

largest overprediction due to neglecting load redistribution from link flexibility. Baseline 2 shows moderate overprediction from ignoring geometric feedback effects as wear evolves.

Table 2 summarizes the predicted RUL statistics, including mean, standard deviation, COV, and prediction error. The proposed model achieves the lowest prediction error (-1.20%) and smallest dispersion (COV: 3.02%), confirming the importance of incorporating both rigid–flexible coupling and geometric feedback for reliable RUL prognostics.

6. Conclusion

This paper presents a physics-informed stochastic framework for wear prediction and RUL assessment in spatial multi-bar linkages. The approach integrates screw theory with FFRF to capture rigid–flexible coupling dynamics and their effects on contact mechanics. A wear evolution scheme based on Archard's law feeds geometric degradation back to joint clearance, while a physics-informed Gamma process quantifies life uncertainty through probabilistic distributions. Validation on an RSSR mechanism demonstrates superior accuracy over baselines neglecting coupling or evolution feedback, achieving low prediction error with reasonable uncertainty bounds. The framework provides probability density functions essential for reliability-based maintenance planning.

Future work will extend the framework to multisite wear interactions in complex linkages, incorporate time dependent reliability analysis. The methodology can be generalized to other degradation modes including fatigue and corrosion.

Acknowledgement

This paper was supported by 2024ZK0422, National Natural Science Foundation of China (Grant nos. 52505049), and the Open Fund of State Key Laboratory of Mechanical Transmission for Advanced Equipment (Grant no. SKLMT-MSKFKT-202421).

References

Archard, J. F. (1953). Contact and rubbing of flat surfaces. *Journal of Applied Physics 24*(8), 981–988.

Dykha, M., V. Dytyniuk, and A. Staryi (2025). Probabilistic approach to assessing tribotechnical reliability indicators of friction units.

Gao, F., J. Li, and G. Sun (2024). Efficient and accurate flexible multibody dynamics modeling for complex spacecraft with integrated control applications. *Acta Astronautica 219*, 818–825.

Karhan, H. and Z. Bingül (2025). Automatic determination of the denavit–hartenberg parameters for the forward kinematics of all serial robots: Novel kinematics toolbox. *Machines 13*(10), 944.

Kolawole, F. O., A. T. Ayeni, S. K. Kolawole, O. S. Kolade, and A. F. Owa (2024). Statistical models for predicting wear and friction coefficient of valve tappet using anova. *Tribology in Industry 46*(2), 210.

Lankarani, H. M. and P. E. Nikravesh (1990). A contact force model with hysteresis damping for impact analysis of multibody systems. *Journal of Mechanical Design 112*(3), 369–376.

Liu, F., J. Luo, J. Mo, C. Gao, and Z. Song (2024). Modeling and analysis of rigid-flexible coupling dynamics of a cable-driven manipulator. *Journal of Mechanical Science and Technology 38*(8), 4377–4384.

Müller, A. (2018). Screw and lie group theory in multibody kinematics: Motion representation and recursive kinematics of tree-topology systems. *Multibody System Dynamics 43*(1), 37–70.

Muratović, E., N. Pervan, A. Muminović, and M. Delić (2024). A contact mechanics model for surface wear prediction of parallel-axis polymer gears. *Polymers 16*(20), 2858.

Murray, R. M., Z. Li, and S. S. Sastry (1994). *A Mathematical Introduction to Robotic Manipulation*. Boca Raton, FL: CRC Press.

Pawlus, P. and R. Reizer (2025). A state of the art on mechanically dominated methods of wear modelling. *Archives of Computational Methods in Engineering*, 1–54.

Shabana, A. A. (1997). *Dynamics of Multibody Systems*. Cambridge, UK: Cambridge University Press.

Springis, G. and I. Boiko (2025). Comparative analysis of wear models for accurate wear predictions. *Lubricants 13*(3), 100.

Sun, J. and H. Hu (2024). Dynamic topology optimization of flexible multibody systems. *Nonlinear Dynamics 112*(14), 11711–11743.

Tang, J., L. Qian, J. Ma, L. Chen, G. Chen, Z. Chen, and W. Huang (2024). Knowledge-dominated and data-driven rigid-flexible coupling dynamics for rotating flexible structure. *Knowledge-Based Systems 296*, 111853.

van Noortwijk, J. M. (2009). A survey of the application of gamma processes in maintenance. *Reliability Engineering & System Safety 94*(1), 2–21.

Zhai, G., H. Xiao, G. Yang, H. Guo, J. Tao, and R. Liu (2023). Rigid-flexible coupling dynamics analysis of multi-output transient deployment mechanism based on ancf. In *ICMD: International Conference on Mechanical Design*, pp. 2369–2388. Springer.